

On Secure UAV-aided ISCC Systems

Hongjiang Lei, Congke Jiang, Ki-Hong Park, Mohamed A. Aboulhassan,
Sen Zhou, and Gaofeng Pan

Abstract—Integrated communication and sensing, which can make full use of the limited spectrum resources to perform communication and sensing tasks simultaneously, is an up-and-coming technology in wireless communication networks. In this work, we investigate the secrecy performance of an uncrewed aerial vehicle (UAV)-assisted secure integrated communication, sensing, and computing system, where the UAV sends radar signals to locate and disrupt potential eavesdroppers while providing offload services to ground users (GUs). Considering the constraints of UAV maximum speed, transmit power, and propulsion energy, as well as secure offloading, data transmission, and computation time, the total energy consumption of GUs is minimized by jointly optimizing user offloading ratio, user scheduling strategy, transmit beamforming, and UAV trajectory. An efficient iterative optimization algorithm is proposed to solve the non-convex optimization problem caused by tightly coupled dependent variables. In particular, the original optimization problem is decomposed into four sub-optimization problems, and the non-convex sub-problems are transformed into approximately convex forms via successive convex approximation. Then, all sub-problems are solved successively by using the block coordinate descent technique. Numerical results demonstrate the convergence and validate the effectiveness of the proposed algorithm.

Index Terms—Integrated sensing, communication, and computing (ISCC), uncrewed aerial vehicle (UAV), mobile edge computing (MEC), physical-layer security (PLS).

I. INTRODUCTION

A. Background and Related Works

Integrated sensing and communication (ISAC) has received extensive attention as an emerging technology that enhances spectral efficiency, energy efficiency, communication performance, and sensing performance by sharing spectral resources and hardware platforms. Moreover, the cooperation of the two functions can also bring integration gains and cooperation gains to the system [1]-[4].

Manuscript received.

This work was supported by the National Natural Science Foundation of China under Grant 62171031 and 61971080. (Corresponding author: Hongjiang Lei.)

Hongjiang Lei and Congke Jiang are with School of Communications and Information Engineering, Chongqing University of Posts and Telecommunications, Chongqing 400065, China, and Chongqing Key Laboratory of Mobile Communications Technology, Chongqing 400065, China (e-mail: leihj@cqupt.edu.cn, cquptjck@163.com).

Ki-Hong Park is with the CEMSE Division, King Abdullah University of Science and Technology (KAUST), Thuwal 23955-6900, Saudi Arabia (e-mail: kihong.park@kaust.edu.sa).

Mohamed A. Aboulhassan is with Electronics and Communications Program, Faculty of Engineering, Alamein International University (AIU), New Alamein City 51718, Egypt (e-mail: maboulhassan@aiu.edu.eg).

Sen Zhou is with Chongqing Academy of Metrology and Quality Inspection, Chongqing, 401121, China (e-mail: cqzhusen@163.com).

Gaofeng Pan is with the School of Cyberspace Science and Technology, Beijing Institute of Technology, Beijing 100081, China (e-mail: gfp-an@bit.edu.c).

Due to the advantages of high mobility and flexible deployment, uncrewed aerial vehicle (UAV)-assisted ISAC systems have been widely studied [5] - [12]. In [7], an adaptive ISAC mechanism for UAVs was proposed, which can adjust the sensing and communication time according to the demand and avoid excessive sensing and resource waste so as to improve resource utilization and system performance. The authors of [8] studied a multi-antenna UAV-ISAC scenario and formulated the minimum-user rate maximization problem and minimum-target detection probability maximization problem, respectively by jointly designing communication precoding, UAV flight trajectory, and sensing precoding. The authors of [9] proposed a periodic sensing and communication framework for UAV-aided ISAC systems, offering enhanced flexibility in balancing the dual functions. Considered the sensing frequency and beam pattern gain requirements for sensing targets, the achievable rate was maximized by jointly optimizing UAV trajectory, user scheduling, sensing target selection and transmit beamforming. Based on real-time communication/sensing performance, a three-stage ISAC scheme with dynamic sensing duration and frequency was proposed in [10]. In the first stage, the initial state of the vehicle was estimated, followed by the use of ISAC wide beams in the second stage to achieve vehicle coverage, the use of extended Kalman filtering (EKF) for state tracking and prediction. In the third stage, the UAV selectively transmitted either an ISAC beam or a communication-only beam according to the monitored sensing and communication performance metrics. In [11], an ISAC-based multi-UAV assisted IoT system was proposed; considering the constraint of radar mutual information, and the minimum communication rate was maximized by designing node scheduling, transmit power, and 3D trajectory of the UAVs. A resource allocation problem of a multi-UAV assisted ISAC system was investigated in [12], and the sum weighted rate of users was maximized by jointly optimizing UAV trajectory, user scheduling, and beamforming design.

With the wide application of ISAC, the amount of data to be processed also increased and integrated sensing, communication, and computing (ISCC) systems was introduced to solve the problem of limited resources [13]. A multi-access ISCC system was investigated in [14], where energy efficiency was maximized by optimizing beamforming for radar sensing and offloading transmission. In [15], a joint communication, sensing, and multi-tier computing system was studied and utilized non-orthogonal multiple access technology to maximize computational offloading capabilities and suppress inter-functionality interference. The authors of [16] investigated an ISCC system where a multi-functional base station (BS) jointly performed downlink communication, target sensing, and edge computing tasks. A weighted sum rate was maximized by

joint optimizing information beamforming, sensing covariance matrix, receiving beamforming, computing resources, and offloading strategy. The application of mobile edge computing (MEC) in a UAV-assisted ISCC system was studied in [17]-[20]. In [17], the authors introduced a tri-functional UAV-assisted ISCC framework, analytically characterizing the Pareto boundary between computational capacity and sensing beam pattern gain, thereby revealing their fundamental trade-off relationship. The authors of [18] addressed the joint optimization problem of communication-sensing precoding matrices and UAV deployment to maximize the weighted sum of sensing and communication performance metrics. In [19], the UAV-assisted ISCC system performed three functions: sensing user devices to obtain radar sensing data, performing computing tasks, and offloading incomplete tasks to the access point (AP) for further processing. The weighted sum energy consumption was minimized by jointly optimizing UAV central processing unit (CPU) frequency, UAV sensing power, user transmission power, and UAV trajectory. The authors of [20] proposed a UAV that was equipped with an edge information hub to perform communication, sensing, and computing systems. Departing from traditional MEC architectures, this edge information hub enables robotic control via closed-loop coordination of sensing, communication, computing, and control functions. The framework simultaneously optimizes multiple control performance indicators while satisfying constraints on satellite backhaul rates, computational capacity, and available onboard energy.

Physical layer security (PLS) is a technology that can improve the information transmission security of ISAC systems [21]. The authors of [22] proposed a UAV-assisted secure ISAC system with multiple users, multiple eavesdropping, and two UAVs. The secrecy rate was maximized by optimizing user scheduling, transmit power, and UAV trajectory. In an intelligent reflecting surface (IRS)-assisted UAV-ISAC network, a secure transmission scheme was proposed to maximize the average achievable rate by jointly designing transmission power allocation, user and sensing target scheduling, IRS phase shift, and UAV trajectory and speed in [23]. In [24], a mobile ground eavesdropper was considered in the UAV-assisted ISAC system. To maximize the real-time secrecy rate, the UAV employed the EKF technique to track and predict the position of the user, and the UAV trajectory was optimized based on the received radar echoes. The authors of [25] considered a UAV-assisted ISAC system with an aerial eavesdropper. The information UAV used the jamming signal and EKF to estimate the position information of the eavesdropping UAV, predict the eavesdropper channel and design the communication resource allocation strategy for the next time slot while communicating with legitimate users.

B. Motivation and Contributions

The performance of the UAV-aided ISCC systems can be significantly improved due to line-of-sight (LoS) dominating the air-to-ground (A2G) channel. In addition, ISAC technology and PLS technology combined with air MEC system exploits UAV flexibility, high mobility, security, low consumption, and

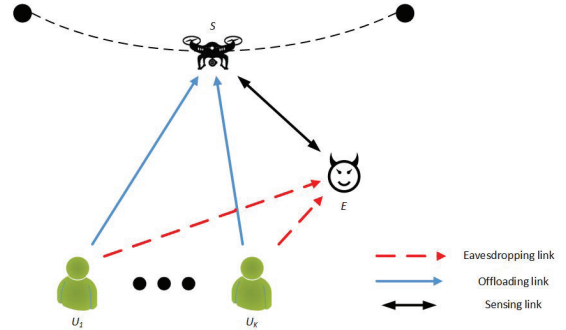


Fig. 1: System model.

other advantages. Through ISAC technology, radar signals are transmitted to locate and interfere with potential eavesdroppers while communicating with ground users, and the limited spectrum resources are used to make communication more secure and efficient. Motivated by this practical significance, an ISAC-based UAV-assisted security MEC system is investigated in this work. The main contributions of this paper are summarized as follows.

- 1) We propose a secure UAV-aided ISCC system. A UAV equipped with an edge server is used as an aerial BS, transmitting radar signals to locate and disrupt potential eavesdroppers while receiving uplink communications from terrestrial users. The user scheduling scheme was utilized to reduce the mutual interference between the users. The users' energy consumption is minimized by jointly optimizing the user offloading ratio, the user scheduling strategy, the sensing beamforming, and the UAV trajectory subject to the constraints of the UAV's starting and ending position, maximum flight speed, transmit power, energy consumption, and the threshold of safe communication and sensing.
- 2) Due to the tight coupling between the optimization variables, solving this non-convex optimization problem is very challenging. Several subproblems of the original problem decomposition are transformed into approximately convex forms by successive convex approximation (SCA) and then solved successively by block coordinate descent (BCD) technology.
- 3) Relative to [22] and [25], wherein the security of UAV-aided systems was investigated, this work maximizes the energy consumption of GUs considered UAV propulsion constraint, which makes the optimization problem more challenging.

II. SYSTEM MODEL AND PROBLEM FORMULATION

As shown in Fig. 1, we consider a UAV-aided ISCC system consisting of K single-antenna users ($U_k, k = 1, 2, \dots, K$) and a UAV (S) works an aerial BS. To reduce the local computation pressure of latency-sensitive users, we assume that they can partially offload their computation tasks to S . A potential terrestrial single-antenna eavesdropper (E) overhears the uplink offloading signals from U_k to S . At the same time, S transmits a radar signal to detect E with a uniform planar array (UPA) with $M = M_x \times M_y$ antennas where M_x and

M_y denote the number of elements along the x - and y - axis, respectively. The adjacent elements are separated by half a wavelength. It is assumed that S flies at a constant altitude H , and the total flight time is represented as T , which is equally divided into N slots, and each slot with a duration of $\delta_t = \frac{T}{N}$ [26], [27]. It is also assumed that S has the location information of U_k , which is expressed as $\mathbf{q}_k = [x_k, y_k]^T$. The coordinate of E is expressed as $\mathbf{q}_e = [x_e, y_e]^T$. In the n -th slot, the horizontal coordinate of S is expressed as $\mathbf{q}_s[n] = [x_s[n], y_s[n]]^T$, and the Euclidean distance from S to the U_k and to E are expressed as $d_{sk}[n] = \sqrt{\|\mathbf{q}_s[n] - \mathbf{q}_k\|^2 + H^2}$ and $d_{se}[n] = \sqrt{\|\mathbf{q}_s[n] - \mathbf{q}_e\|^2 + H^2}$, respectively.

A. Communication and Sensing Model

Similar to [28], the ground-to-ground (G2G) channel between E and U_k is characterized as Rayleigh fading model, which is expressed as

$$h_{ek} = \sqrt{\frac{\beta_0}{\|\mathbf{q}_k - \mathbf{q}_e\|^2}} \tilde{h}_{ek} \quad (1)$$

where β_0 denotes the reference channel gain at 1 meter and $\tilde{h}_{ek} \sim \mathcal{CN}(0, 1)$.

Similar to [29] and [30], we assume that the A2G channel between S and users and E is an LoS link. In the n -th slot, the channel from S to U_k and E are expressed as

$$h_{sk}[n] = \sqrt{\frac{\beta_0}{d_{sk}^2[n]}} \quad (2)$$

and

$$\mathbf{h}_{se}[n] = \sqrt{\frac{\beta_0}{d_{se}^2[n]}} \mathbf{a}_{se}^H[n], \quad (3)$$

respectively. The round-trip channel between S and E is given by [31]

$$\mathbf{h}_{ses}[n] = \sqrt{\frac{\beta_0 \xi}{d_{se}^4[n]}} \mathbf{a}_{se}^H[n] \quad (4)$$

where ξ denotes the radar cross-section, $\mathbf{a}_{se}^H[n] = [1, e^{j\pi\Phi_e[n]}, \dots, e^{j\pi(M_x-1)\Phi_e[n]}] \otimes [1, e^{j\pi\Omega_e[n]}, \dots, e^{j\pi(M_y-1)\Omega_e[n]}]$ signifies the response vector of S antenna array, $\Phi_e[n] = \frac{x_s[n] - x_e}{d_{se}[n]}$, and $\Omega_e[n] = \frac{y_s[n] - y_e}{d_{se}[n]}$ [9].

For fair data offloading among users during the S flight, a binary variable $\theta_k(n)$ is employed to represent the scheduling decision, where $\theta_k(n) = 1$ denotes that U_k is allocated to communicate with S in the n -th time slot. Thus, we have

$$\sum_{k=1}^K \theta_k(n) \leq 1, \forall n, \quad (5)$$

$$\theta_k(n) \in \{0, 1\}, \forall n, k. \quad (6)$$

The received signal by S is expressed as

$$y_{sk}[n] = \sum_{k=1}^K \theta_k[n] h_{sk}[n] s_k[n] + \mathbf{h}_{ses}[n] \mathbf{w}[n] s_{se} + n_s \quad (7)$$

where $s_k \in \mathcal{CN}(0, 1)$ represents the uplink offloading signal from U_k to S , $s_{se} \in \mathcal{CN}(0, 1)$ denotes the radar symbol, $\mathbf{w}[n] \in \mathbb{C}^{M \times 1}$ denotes the precoding vector for detecting, $n_s \in \mathcal{CN}(0, \sigma_s^2)$ denotes additive white Gaussian noise (AWGN) at S . Then, the signal-to-interference-plus-noise ratio (SINR) of S is obtained as

$$\gamma_{sk}[n] = \frac{P_u \theta_k[n] |h_{sk}[n]|^2}{\mathbf{h}_{ses}[n] \mathbf{W}[n] \mathbf{h}_{ses}^H[n] + \sigma_s^2} \quad (8)$$

where $\mathbf{W}[n] = \mathbb{E}\{\mathbf{w}[n] \mathbf{w}^H[n]\}$ and P_u denotes the transmit power of U_k . The offloading rate is expressed as

$$R_{sk}[n] = \log_2 \left(1 + \frac{P_u \theta_k[n] |h_{sk}[n]|^2}{\mathbf{h}_{ses}[n] \mathbf{W}[n] \mathbf{h}_{ses}^H[n] + \sigma_s^2} \right). \quad (9)$$

The received signal by E is expressed as

$$y_{ek}[n] = \sum_{k=1}^K \theta_k[n] h_{ek}[n] s_k[n] + \mathbf{h}_{se}[n] \mathbf{w}[n] s_{se} + n_e \quad (10)$$

where $n_e \in \mathcal{CN}(0, \sigma_e^2)$ denotes AWGN at E . The SINR for E to wiretap the signal from U_k is obtained as

$$\gamma_{ek}[n] = \frac{P_u \theta_k[n] |h_{ek}[n]|^2}{\mathbf{h}_{se}[n] \mathbf{W}[n] \mathbf{h}_{se}^H[n] + \sigma_e^2}. \quad (11)$$

It must be noted that since h_{ek} is a random variable, $\gamma_{ek}[n]$ is a random variable. Thus, with the method in Refs. [32] and [33], $\gamma_{ek}[n]$ is approximated as

$$\bar{\gamma}_{ek} = \frac{P_u \theta_k[n] \mathbb{E}\{|h_{ek}[n]|^2\}}{\mathbf{h}_{se}[n] \mathbf{W}[n] \mathbf{h}_{se}^H[n] + \sigma_e^2} \quad (12)$$

$$= \frac{P_u \theta_k[n] \beta_0}{(\mathbf{h}_{se}[n] \mathbf{W}[n] \mathbf{h}_{se}^H[n] + \sigma_e^2) \|\mathbf{q}_k - \mathbf{q}_e\|^2}. \quad (13)$$

The eavesdropping rate of E is

$$R_{ek}[n] = \log_2(1 + \bar{\gamma}_{ek}). \quad (14)$$

The transmit beampattern gain from S to E is expressed as [34], [35]

$$P[n] = \mathbf{a}_{se}^H[n] \mathbf{W}[n] \mathbf{a}_{se}[n]. \quad (15)$$

To meet the requirement of detecting, the following constraint should be satisfied [36],

$$P[n] \geq d_{se}^2[n] \Gamma_{\text{sen}}, \forall n \quad (16)$$

where Γ_{sen} is a perceived threshold.

B. Computing Model

We assume that U_k has D_k (bit) computational task in total and these data can be divided into any amount of data to deal with. All the tasks are required to be completed within S flight time T . Like [37], since the data of the computation result is very small, the delay and energy consumption of back transmission can be ignored. In the n -th time slot, we define $\alpha_k[n] \in [0, 1]$ as the proportion of data offloaded by U_k , which signifies that $\sum_{n=1}^N \alpha_k[n] \leq 1, \forall k$. Thus the proportion

computation locally at U_k is expressed as $1 - \sum_{n=1}^N \theta_k [n] \alpha_k [n]$. The computing time and energy consumption at U_k are given by [38]

$$T_k^{\text{loc}} = \left(1 - \sum_{n=1}^N \theta_k [n] \alpha_k [n]\right) D_k F_k / f_k \quad (17)$$

and

$$E_k^{\text{loc}} = \kappa \left(1 - \sum_{n=1}^N \theta_k [n] \alpha_k [n]\right) D_k F_k f_k^2 \quad (18)$$

where F_k (cycles/bit) is the required CPU cycles per bit at U_k , f_k (cycles/s) represents the local computing capacity for the task at U_k , and κ denotes the energy efficiency coefficient of the CPU at U_k [36].

The time and the offloading energy consumption required for the U_k in slot n are expressed as

$$T_k^{\text{offload}} [n] = \frac{\theta_k [n] \alpha_k [n] D_k}{B \hat{R}_{sk} [n]} \quad (19)$$

and

$$E_k^{\text{offload}} [n] = \frac{P_u \theta_k [n] \alpha_k [n] D_k}{B \hat{R}_{sk} [n]} \quad (20)$$

respectively, where B denotes the channel bandwidth and $\hat{R}_{sk} [n] = \log_2 \left(1 + \frac{P_u |h_{sk} [n]|^2}{\mathbf{h}_{ses} [n] \mathbf{W} [n] \mathbf{h}_{es}^H [n] + \sigma_s^2}\right)$. The time and energy consumption at S to deal with the offloaded data from U_k in the n -th time slot are expressed as

$$T_k^{\text{com}} [n] = \alpha_k [n] D_k F_s / f_s \quad (21)$$

and

$$E_k^{\text{com}} [n] = \kappa \alpha_k [n] D_k F_s f_s^2, \quad (22)$$

respectively, where F_s (cycles/bit) is the required CPU cycles per bit and f_s (cycles/s) represents the local computing capacity for the task at S .

To ensure that data offloaded in the n -th time slot can be fully deal with, the following constraint must be satisfied [20], [40],

$$(T_k^{\text{offload}} [n] + T_k^{\text{com}} [n]) \theta_k [n] \leq \delta_t, \forall n, k. \quad (23)$$

The total energy consumption of U_k and S are expressed as

$$E_k = E_k^{\text{loc}} + \sum_{n=1}^N \theta_k [n] E_k^{\text{offload}} [n] \quad (24)$$

and

$$E_S = E_{\text{fly}} + E_{\text{sen}} + \sum_{k=1}^K \sum_{n=1}^N \theta_k [n] E_k^{\text{com}} [n], \quad (25)$$

respectively, where $E_{\text{sen}} = \sum_{n=1}^N \delta_t \text{tr}(\mathbf{W} [n])$ and $E_{\text{fly}} = \sum_{n=1}^N \delta_t P_{\text{fly}} [n]$ denote the energy consumption for sensing and

and propulsion, respectively, the propulsion power of S is expressed as [41]

$$P_{\text{fly}} [n] = P_i \left(\sqrt{1 + \frac{v^4 [n]}{4v_0^4}} - \frac{v^2 [n]}{2v_0^2} \right)^{\frac{1}{2}} + \frac{1}{2} d_0 \rho s A v^3 [n] + P_0 \left(1 + \frac{3v^2 [n]}{U_{\text{tip}}^2} \right), \forall n \quad (26)$$

where $v [n] = \frac{\|\mathbf{q}_s [n+1] - \mathbf{q}_s [n]\|}{\delta_t}$ denotes the speed of UAV, P_0 and P_i denote the blade profile and the induced power in hover state, U_{tip} signifies the tip velocity of the rotor blade, v_0 denotes the mean rotor induced speed in hover, d_0 , ρ , s , and A represent the drag ratio of the fuselage, the air density, solidity of the rotor and rotor disc area, respectively.

C. Problem Formulation

In this work, the total energy consumption for all users is minimized with respect to the user offloading ratio, the user scheduling, the transmit beamforming, and UAV trajectory. Let $\mathbf{A} = \{\alpha_k [n], \forall k, n\}$, $\mathbf{B} = \{\theta_k [n], \forall k, n\}$, $\mathbf{W} = \{\mathbf{w} [n], \forall n\}$ and $\mathbf{Q}_s = \{\mathbf{q}_s [n], \forall n\}$. Therefore, we have the following optimization problem,

$$\mathcal{P}_0 : \min_{\mathbf{A}, \mathbf{B}, \mathbf{W}, \mathbf{Q}_s} \sum_{k=1}^K E_k \quad (27a)$$

$$\text{s.t. } \theta_k [n] \in \{0, 1\}, \forall k, n \quad (27b)$$

$$\sum_{k=1}^K \theta_k [n] \leq 1, \forall n \quad (27c)$$

$$\alpha_k [n] \in [0, 1], \forall k, n \quad (27d)$$

$$\sum_{n=1}^N \alpha_k [n] \leq 1, \forall k \quad (27e)$$

$$\mathbf{q}_s [1] = \mathbf{q}_s^0, \mathbf{q}_s [N] = \mathbf{q}_s^F \quad (27f)$$

$$\|\mathbf{q}_s [n+1] - \mathbf{q}_s [n]\| \leq \delta_t V_{\text{max}}, \forall n \quad (27g)$$

$$\gamma_{sk} [n] \geq \theta_k [n] \Gamma_s, \forall k, n \quad (27h)$$

$$\bar{\gamma}_{ek} [n] \leq \theta_k [n] \Gamma_e, \forall k, n \quad (27i)$$

$$\text{tr}(\mathbf{W} [n]) \leq P_{\text{max}}, \forall n \quad (27j)$$

$$E_S \leq E_{\text{max}} \quad (27k)$$

$$(16), (23) \quad (27l)$$

where \mathbf{q}_s^0 and \mathbf{q}_s^F signify the initial position and the final position of S , respectively, V_{max} denotes the maximum velocity of S , Γ_s and Γ_e denote the threshold for communication, eavesdropping, respectively, and Γ_{sen} denotes the threshold for sensing, P_{max} denotes the maximum transmitting power of S , and E_{max} is S 's battery capacity. (27b) and (27c) are the user scheduling constraints, (27d) and (27e) are the constraints on offloading ratio, (27f) and (27g) denote constraints on trajectory of S , (27h) and (27i) represent the requirements of secure communication, (27j) signifies the constraint on transmission power in each time slot, and (27k) represents the total energy of UAV constraint.

It can be observed that \mathcal{P}_0 is difficult to solve by the traditional algorithm. First, the objective function is a function

of \mathbf{A} , \mathbf{B} , $\tilde{\mathbf{W}}$, and \mathbf{Q}_s , which is too complex to determine the concavity and convexity. Second, (16), (23), (27h) and (27i) are non-convex since the strong coupling of $\tilde{\mathbf{W}}$ and \mathbf{Q}_s . Third, the non-convexity of (27k) stems from the complexity of E_s , which violates the convexity constraint. Consequently, directly solving the original problem \mathcal{P}_0 proves to be mathematically intractable.

III. PROPOSED SOLUTION

To solve \mathcal{P}_0 , alternating optimization method is utilized to optimize the user offloading ratio \mathbf{A} , the user scheduling \mathbf{B} , transmit beamforming $\tilde{\mathbf{W}}$, and S trajectory \mathbf{Q}_s in an alternating way, by considering the others to be given.

A. Subproblem 1: Offloading Proportion Optimization

In this subsection, \mathbf{A} is optimized with given $\{\mathbf{B}, \tilde{\mathbf{W}}, \mathbf{Q}_s\}$. \mathcal{P}_0 is rewritten as

$$\begin{aligned} \mathcal{P}_{1.1} : \min_{\mathbf{A}} \sum_{k=1}^K E_k \quad (28a) \\ \text{s.t. (23), (27d), (27e).} \end{aligned}$$

$\mathcal{P}_{1.1}$ is a linear programming (LP), which can be solved by existing optimization tools such as CVX.

B. Subproblem 2: User Scheduling Optimization

In this subsection, \mathbf{B} is optimized with given $\{\mathbf{A}, \tilde{\mathbf{W}}, \mathbf{Q}_s\}$. Firstly, like [26], $\theta_k[n]$ is relaxed into a continuous variable, ranging from 0 to 1, to restrain this binary constraint. Then, \mathcal{P}_0 is expressed as

$$\begin{aligned} \mathcal{P}_{2.1} : \min_{\mathbf{B}} \sum_{k=1}^K E_k \quad (29a) \\ \text{s.t. (23), (27b), (27c), (27h), (27i).} \end{aligned}$$

$\mathcal{P}_{2.1}$ is a linear programming problem, which can be solved by CVX.

C. Subproblem 3: Transmit Beamforming Optimization

In this subsection, $\tilde{\mathbf{W}}$ is optimized with given $\{\mathbf{A}, \mathbf{B}, \mathbf{Q}_s\}$. Based on (24), one can find that E_k^{loc} is a constant for given \mathbf{A} and \mathbf{B} . Thus, \mathcal{P}_0 is rewritten as

$$\begin{aligned} \mathcal{P}_{3.1} : \min_{\tilde{\mathbf{W}}} \sum_{k=1}^K \sum_{n=1}^N \theta_k[n] E_k^{\text{offload}}[n] \quad (30a) \\ \text{s.t. } \mathbf{W}[n] \geq 0 \quad (30b) \\ \text{rank}(\mathbf{W}[n]) = 1 \quad (30c) \\ (16), (23), (27h) - (27j). \end{aligned}$$

It should be noted that the objective function is non-convex with respect to $\tilde{\mathbf{W}}[n]$. To solve it, a slack variable $\eta_k[n]$ is introduced which is satisfied the following constraint

$$\eta_k[n] \geq \theta_k[n] E_k^{\text{offload}}[n] = \frac{P_u c_k[n]}{\hat{R}_{sk}[n]} \quad (31)$$

where $c_k[n] = \frac{\theta_k[n] \alpha_k[n] D_k}{B}$. Moreover, $\hat{R}_{sk}[n]$ is rewritten as $\hat{R}_{sk}[n] = \log_2 \left(1 + \frac{P_u |h_{sk}[n]|^2}{X_{w1}[n]} \right)$, where $X_{w1}[n] = \mathbf{h}_{ses}[n] \mathbf{W}[n] \mathbf{h}_{ses}^H[n] + \sigma_s^2$. We rewrite (31) as

$$\hat{R}_{sk}[n] \geq \frac{P_u c_k[n]}{\eta_k[n]}. \quad (32)$$

It should be noted that (32) is non-convex with respect to $\tilde{\mathbf{W}}$ since the left-hand side of it is convex but not concave. To tackle this problem, the first-order Taylor expansion is utilized to transform (32) into (33), shown at the top of the next page, where $(\cdot)^{(m)}$ denotes a given feasible point in the m th iteration.

By ignoring the rank-one constraint, $\mathcal{P}_{3.1}$ is converted to

$$\mathcal{P}_{3.2} : \min_{\tilde{\mathbf{W}}, \eta_k[n]} \sum_{k=1}^K \sum_{n=1}^N \eta_k[n] \quad (34a)$$

$$\text{s.t. } \mathbf{W}[n] \geq 0 \quad (34b)$$

$$\eta_k[n] \geq 0 \quad (34c)$$

$$(16), (23), (27h) - (27j), (33).$$

$\mathcal{P}_{3.2}$ is a semidefinite programming problem (SDP), which can be solved with CVX. Subsequently, some technologies, such as the Gaussian randomization, singular value decomposition, or the similar method proposed in [42], can be utilized to solve the rank-one constraint.

D. Subproblem 4: Trajectory of UAV Optimization

In this subsection, \mathbf{Q}_s is optimized with given $\{\mathbf{A}, \mathbf{B}, \tilde{\mathbf{W}}\}$. Similarly, \mathcal{P}_0 is rewritten as

$$\mathcal{P}_{4.1} : \min_{\mathbf{Q}_s, \tau_k[n]} \sum_{k=1}^K \sum_{n=1}^N \tau_k[n] \quad (35a)$$

$$\text{s.t. } \tau_k[n] \geq \theta_k[n] E_k^{\text{offload}}[n] \quad (35b)$$

$$(16), (23), (27f) - (27i), (27k)$$

where $\tau_k[n]$ is a slack variable. It should be noted that $\mathcal{P}_{4.1}$ is a non-convex problem since (16), (23), (27h), (27i), (27k), and (35b) are non-convex constraints.

Firstly, (16) is rewritten as

$$P[n] = \mathbf{a}_{se}^H[n] \mathbf{W}[n] \mathbf{a}_{se}[n] \geq d_{se}^2[n] \Gamma_{\text{sen}}. \quad (36)$$

It should be noted that the left-hand side of (36) is non-concave and the right-hand side of (36) ($d_{se}^2[n]$) is non-convex with respect to \mathbf{Q}_s . To solve the problem, the first order Taylor expansion is utilized. Then we have

$$\begin{aligned} \tilde{d}_{se}[n] = 2(\mathbf{q}_s^m[n] - \mathbf{q}_e)^T (\mathbf{q}_s[n] - \mathbf{q}_s^m[n]) \\ + \|\mathbf{q}_s^m[n] - \mathbf{q}_e\|^2 + H^2 \end{aligned} \quad (37)$$

and

$$\tilde{\mathbf{a}}_{se}^H[n] = (\mathbf{a}_{se}^H[n])^{(m)} + (\mathbf{q}_s[n] - \mathbf{q}_s^m[n])^T \dot{\mathbf{a}}_{se}[n] \quad (38)$$

where $\dot{\mathbf{a}}_{se}[n] = \left[\frac{\partial(\mathbf{a}_{se}^H[n])^{(m)}}{\partial x_s[n]}, \frac{\partial(\mathbf{a}_{se}^H[n])^{(m)}}{\partial y_s[n]} \right]$, $\frac{\partial(\mathbf{a}_{se}^H[n])^{(m)}}{\partial x_s[n]}$ and $\frac{\partial(\mathbf{a}_{se}^H[n])^{(m)}}{\partial y_s[n]}$ are given in (39) and (40), respectively, shown at the top of this page, where $\mathbf{a}_x^H[n]$, $\mathbf{a}_y^H[n]$,

$$\log_2 \left(1 + \frac{P_u |h_{sk}[n]|^2}{X_{w1}^{(m)}[n]} \right) - \frac{P_u |h_{sk}[n]|^2 (X_{w1}[n] - X_{w1}^{(m)}[n])}{\ln 2 \left((X_{w1}^{(m)}[n])^2 + X_{w1}^{(m)}[n] P_u |h_{sk}[n]|^2 \right)} \geq \frac{P_u c_k[n]}{\eta_k[n]} \quad (33)$$

$$\frac{\partial (\mathbf{a}_{se}^H[n])^{(m)}}{\partial x_s[n]} = \left[0, -j\pi\Phi_{ex}^{(m)}[n] \cdots, -(M_x - 1)j\pi\Phi_{ex}^{(m)}[n] \right] \odot \mathbf{a}_x^H[n] \otimes \mathbf{a}_y^H[n] + \mathbf{a}_x^H[n] \otimes \left(\mathbf{a}_y^H[n] \odot \left[0, -j\pi\Omega_{ex}^{(m)}[n] \cdots, -(M_y - 1)j\pi\Omega_{ex}^{(m)}[n] \right] \right) \quad (39)$$

$$\frac{\partial (\mathbf{a}_{se}^H[n])^{(m)}}{\partial y_s[n]} = \left[0, -j\pi\Phi_{ey}^{(m)}[n] \cdots, -(M_x - 1)j\pi\Phi_{ey}^{(m)}[n] \right] \odot \mathbf{a}_x^H[n] \otimes \mathbf{a}_y^H[n] + \mathbf{a}_x^H[n] \otimes \left(\mathbf{a}_y^H[n] \odot \left[0, -j\pi\Omega_{ey}^{(m)}[n] \cdots, -(M_y - 1)j\pi\Omega_{ey}^{(m)}[n] \right] \right) \quad (40)$$

$$\mathbf{a}_x^H[n] = \left[1, e^{-j\pi\Phi_e^{(m)}[n]}, \dots, e^{-j\pi(M_x-1)\Phi_e^{(m)}[n]} \right], \mathbf{a}_y^H[n] = \left[1, e^{-j\pi\Omega_e^{(m)}[n]}, \dots, e^{-j\pi(M_y-1)\Omega_e^{(m)}[n]} \right] \quad (41)$$

$$\Phi_{ex}^{(m)}[n] = \frac{(y_s^{(m)}[n] - y_e)^2 + H^2}{l_{se}^{(m)}[n]}, \Phi_{ey}^{(m)}[n] = \frac{-(y_s^{(m)}[n] - y_e)^2}{l_{se}^{(m)}[n]} \quad (42)$$

$$\Omega_{ex}^{(m)}[n] = \frac{-(x_s^{(m)}[n] - x_e)^2}{l_{se}^{(m)}[n]}, \Omega_{ey}^{(m)}[n] = \frac{(x_s^{(m)}[n] - x_e)^2 + H^2}{l_{se}^{(m)}[n]} \quad (43)$$

$$\tilde{P}[n] = (\tilde{\mathbf{a}}_{se}^H[n])^{(m)} \mathbf{W}[n] (\tilde{\mathbf{a}}_{se}[n])^{(m)} + 2(\tilde{\mathbf{a}}_{se}^H[n])^{(m)} \mathbf{W}[n] (\tilde{\mathbf{a}}_{se}[n] - (\tilde{\mathbf{a}}_{se}[n])^{(m)}) \quad (44)$$

$\Phi_{ex}^{(m)}[n]$, $\Phi_{ey}^{(m)}[n]$, $\Omega_{ex}^{(m)}[n]$, and $\Omega_{ey}^{(m)}[n]$, are given as (41) - (43), respectively, and $l_{se}^{(m)}[n] =$

$\sqrt{\left((x_s^{(m)}[n] - x_e)^2 + (y_s^{(m)}[n] - y_e)^2 + H^2 \right)^3}$. As

$P[n] = \tilde{\mathbf{a}}_{se}^H[n] \mathbf{W}[n] \tilde{\mathbf{a}}_{se}[n]$ is a non-linear, (44) is approximated via the first-order Taylor approximation similarly, which shown at the top of the next page. Then, (16) is approximated as

$$\tilde{P}[n] \geq \tilde{d}_{se}[n] \Gamma_{sen}. \quad (45)$$

Secondly, (23) is rewritten as

$$M_k[n] \left(\sigma_s^2 \tilde{d}_{sk}[n] + \frac{\beta_0 \xi P[n] \tilde{d}_{sk}[n]}{(\tilde{d}_{se}[n])^2} \right) \leq \theta_k[n] P_u \beta_0 \quad (46)$$

where $M_k[n] = \left(2^{\frac{c_k[n]}{(\delta_t - T_k^{\text{com}}[n])\theta_k[n]}} - 1 \right)$ and $\tilde{d}_{sk}[n] =$

$2(\mathbf{q}_s^m[n] - \mathbf{q}_k)^T (\mathbf{q}_s[n] - \mathbf{q}_s^m[n]) + \|\mathbf{q}_s^m[n] - \mathbf{q}_k\|^2 + H^2$. Since the second term inside the left-hand side of (46) contains the multiplication of three variables, making this constraint non-convex, it is expanded by a single Taylor to introduce the

auxiliary variable $X_1[n]$ in (47), which is displayed at the top of the next page. Then, (23) is rewritten as

$$M_k[n] \left(\sigma_s^2 \tilde{d}_{sk}[n] + X_1[n] \right) \leq \theta_k[n] P_u \beta_0. \quad (48)$$

With the same method of (23), (27h) and (27i) are rewritten as

$$\theta_k[n] \left(\sigma_s^2 \tilde{d}_{sk}[n] + X_1[n] \right) \leq \frac{\theta_k[n] P_u \beta_0}{\Gamma_s} \quad (49)$$

and

$$\theta_k[n] \left(\frac{P_u |h_{ek}|^2}{\Gamma_e} - \sigma_e^2 \right) \tilde{d}_{se}[n] \leq \theta_k[n] \beta_0 \tilde{P}[n], \quad (50)$$

respectively.

With the same method of (32), (35b) is expressed as

$$\frac{P_u c_k[n]}{\tau_k[n]} \leq \hat{R}_{sk}[n]. \quad (51)$$

This constraint is non-convex since the right-hand side is non-concave. By applying SCA, (51) is rewritten as

$$\log_2 (X_2[n] + \sigma_s^2) - X_3[n] \geq \frac{P_u c_k[n]}{\tau_k[n]} \quad (52)$$

$$\begin{aligned}
X_1[n] &= \frac{\beta_0 \xi P^{(m)}[n] \tilde{d}_{sk}^{(m)}[n]}{\left(\tilde{d}_{se}^{(m)}[n]\right)^2} + \frac{\beta_0 \xi \tilde{d}_{sk}^{(m)}[n]}{\left(\tilde{d}_{se}^{(m)}[n]\right)^2} \left(P[n] - P^{(m)}[n]\right) + \\
&\frac{\beta_0 \xi P^{(m)}[n]}{\left(\tilde{d}_{se}^{(m)}[n]\right)^2} \left(\tilde{d}_{sk}[n] - \tilde{d}_{sk}^{(m)}[n]\right) - \frac{2\beta_0 \xi P^{(m)}[n] \tilde{d}_{sk}^{(m)}[n]}{\left(\tilde{d}_{se}^{(m)}[n]\right)^3} \left(\tilde{d}_{se}[n] - \tilde{d}_{se}^{(m)}[n]\right)
\end{aligned} \tag{47}$$

$$\begin{aligned}
X_2[n] &= \frac{\beta_0 \xi P^{(m)}[n]}{\left(\tilde{d}_{se}^{(m)}[n]\right)^2} + \frac{P_u \beta_0}{\tilde{d}_{sk}^{(m)}[n]} + \frac{\beta_0 \xi}{\left(\tilde{d}_{se}^{(m)}[n]\right)^2} \left(P[n] - P^{(m)}[n]\right) - \\
&\frac{2\beta_0 \xi P^{(m)}[n]}{\left(\tilde{d}_{se}^{(m)}[n]\right)^3} \left(\tilde{d}_{se}[n] - \tilde{d}_{se}^{(m)}[n]\right) - \frac{P_u \beta_0}{\left(\tilde{d}_{sk}^{(m)}[n]\right)^2} \left(\tilde{d}_{sk}[n] - \tilde{d}_{sk}^{(m)}[n]\right)
\end{aligned} \tag{53}$$

$$X_3[n] = \log_2 \left(\frac{\beta_0 \xi P^{(m)}[n]}{\left(\tilde{d}_{se}^{(m)}[n]\right)^2} + \sigma_s^2 \right) + \frac{\frac{\beta_0 \xi}{\left(\tilde{d}_{se}^{(m)}[n]\right)^2} \left(P[n] - P^{(m)}[n]\right) - \frac{2\beta_0 \xi P^{(m)}[n]}{\left(\tilde{d}_{se}^{(m)}[n]\right)^3} \left(\tilde{d}_{se}[n] - \tilde{d}_{se}^{(m)}[n]\right)}{\ln 2 \left(\frac{\beta_0 \xi P^{(m)}[n]}{\left(\tilde{d}_{se}^{(m)}[n]\right)^2} + \sigma_s^2 \right)} \tag{54}$$

$$\begin{aligned}
&\left(v_2^{(m)}[n]\right)^2 + 2v_2^{(m)}[n] \left(v_2[n] - v_2^{(m)}[n]\right) + \frac{\left\| \mathbf{q}_s^{(m)}[n+1] - \mathbf{q}_s^{(m)}[n] \right\|^2}{v_0^2 \delta_t^2} \\
&+ \frac{2}{v_0^2 \delta_t^2} \left(\mathbf{q}_s^{(m)}[n+1] - \mathbf{q}_s^{(m)}[n] \right)^T \left(\mathbf{q}_s[n+1] - \mathbf{q}_s[n] - \mathbf{q}_s^{(m)}[n+1] + \mathbf{q}_s^{(m)}[n] \right) \geq \frac{1}{v_2^2[n]}
\end{aligned} \tag{58}$$

where $X_2[n]$ and $X_3[n]$ are the introduced auxiliary variables, shown at the top of the page respectively.

To deal with (27k), $P_{\text{fly}}[n]$ is approximated as

$$\begin{aligned}
\hat{P}_{\text{fly}}[n] &= P_i v_2[n] + \frac{1}{2} d_0 \rho s A v_1^3 [n] \\
&+ P_0 \left(1 + \frac{3v_1^2 [n]}{U_{\text{tip}}^2} \right)
\end{aligned} \tag{55}$$

where v_1 and v_2 are slack variables that satisfy the following constraints, respectively

$$v_1[n] \geq \frac{\left\| \mathbf{q}_s[n+1] - \mathbf{q}_s[n] \right\|}{\delta_t} \tag{56}$$

and

$$v_2^2[n] + \frac{\left\| \mathbf{q}_s[n+1] - \mathbf{q}_s[n] \right\|^2}{v_0^2 \delta_t^2} \geq \frac{1}{v_2^2[n]}. \tag{57}$$

It should be noted that (57) is non-convex because the left-hand side is convex. With the SCA technology, (57) is approximated as (58), shown at the top of the next page. Then, (27k) is rewritten as

$$\begin{aligned}
&\sum_{n=1}^N \delta_t \hat{P}_{\text{fly}}[n] + \sum_{n=1}^N \delta_t \text{tr}(\mathbf{W}[n]) \\
&+ \sum_{k=1}^K \sum_{n=1}^N E_k^{\text{com}}[n] \leq E_{\text{max}}.
\end{aligned} \tag{59}$$

Finally, $\mathcal{P}_{4.1}$ is reformulated as

$$\begin{aligned}
\mathcal{P}_{4.2} : \min_{\Xi} &\sum_{k=1}^K \sum_{n=1}^N \tau_k [n] \\
\text{s.t.} &(27\text{f}), (27\text{g}), (45), (48), (49), \\
&(50), (52), (56), (58), (59)
\end{aligned} \tag{60a}$$

where $\Xi = \{\mathbf{q}_s[n], \tau_k[n], v_1[n], v_2[n]\}$.

$\mathcal{P}_{4.2}$ is a convex problem and can be solved by existing optimization tools such as CVX.

IV. NUMERICAL RESULTS AND ANALYSIS

In this section, numerical results are given to evaluate the performance achieved by the proposed algorithm. The detailed parameter configurations are summarized in TABLE I. In order to verify the superiority of the proposed algorithm, three benchmarks are given for comparison:

- 1) Benchmark 1: Similar to [7], the user offloading ratio, user scheduling, and transmit beamforming are jointly optimized while S flies with fixed trajectory.
- 2) Benchmark 2: The user offloading ratio and user scheduling are fixed and the transmit beamforming and S trajectory are optimized, similar to [43].
- 3) Benchmark 3: There is no radar signal to interfere with E and the user offloading ratio, user scheduling strategy and S trajectory are optimized, similar to [12]¹.

¹In this scheme, it is assumed that the location of E is known at S .

TABLE I: Simulation Parameters

Notation	Value	Notation	Value
H	50 m	B	10^6 Hz
P_{\max}	30 dBm	D_k	10^7 bit
T	40 s	F_k, F_s	1000 cycles/bit
δ_t	1s	f_k, f_s	0.1 GHz, 10 GHz
M	$4 * 4$	P_0	79.86 W
σ_s^2, σ_e^2	-90 dBm	P_i	88.63 W
$\Gamma_s, \Gamma_e, \Gamma_{sen}$	$1, 0.1, 10^{-5}$	U_{tip}	120 m/s
ξ	1	v_0	4.03 m/s
κ	10^{-26}	d_0	0.6
β_0	-30 dB	ρ	1.225 kg/m^3
E_{\max}	50000 j	s	0.05 m^3
ϵ	0.001	A	0.503 m^2

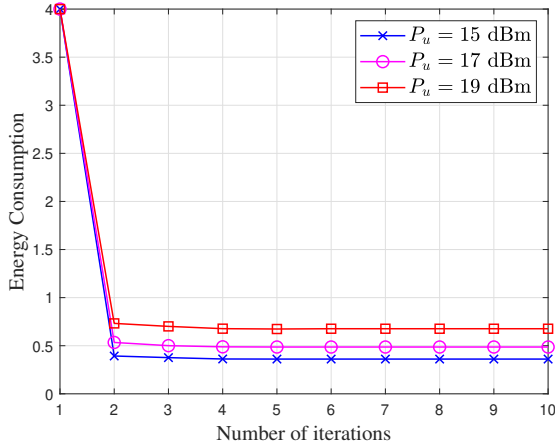


Fig. 2: The user energy consumption versus the number of iterations for different user transmit power.

To testify the robustness of the proposed scheme, the following scenarios are considered

- Scenario 1: The UAV flies from $\mathbf{q}_s^0 = [0, 0]^H$ m to $\mathbf{q}_s^F = [200, 200]^H$ m with $V_{\max} = 8\text{m/s}$. The E is located at $[100, 100]^H$ m, and the positions of the four users are $[50, 25]^H$ m, $[100, 40]^H$ m, $[150, 70]^H$ m and $[175, 150]^H$ m, all on one side of E .
- Scenario 2: The UAV flies from $\mathbf{q}_s^0 = [0, 0]^H$ m to $\mathbf{q}_s^F = [200, 0]^H$ m with $V_{\max} = 8\text{m/s}$. The E is located at $[100, 40]^H$ m, and the positions of the four users are $[20, 20]^H$ m, $[60, 120]^H$ m, $[140, 120]^H$ m and $[180, 20]^H$ m, located around E .
- Scenario 3: The UAV starts from $[20, 100]^H$ m and travels one week counterclockwise back to $[20, 100]^H$ m with $V_{\max} = 15\text{m/s}$. E is located at $[140, 80]^H$ m, and the positions of the four users are $[40, 40]^H$ m, $[160, 40]^H$ m, $[160, 160]^H$ m and $[40, 160]^H$ m.

Fig. 2 shows the convergence of the proposed scheme versus the number of iterations with different transmission power. The results demonstrate the proposed scheme converge rapidly. In particular, one can observe that the users' energy consumption decreases rapidly in the first few iterations and converges after ten iterations. In addition, as the user's transmission power increases, the user's energy consumption also increases.

Figs. 3-5 show the optimized S trajectory, user offloading ratio, and users' energy consumption corresponding to various transmission powers in different scenarios, respectively. In scenario 1 shown in Fig. 3, the users are distributed on the same side of E , and U_2 and U_3 are close to E , while U_1 and U_4 are far from E . It can be observed from Fig. 3(a), in the proposed scheme, when S provides services for users (U_1 and U_4) who are farther away from E , S will be as close to the users as possible. However, when S provides services to users (U_2 and U_3) that are closer to E , S prefers to be closer to E to improve the interference to E . Benchmark 2 has a similar result. In Benchmark 3, S goes directly to U_4 after communicating with U_1 because U_2 and U_3 are too close to E , resulting in a lower security rate. Fig. 3(b) shows the offloading ratio with different schemes. It can be observed that U_1 and U_4 are all offloaded in all the schemes, while the data of U_2 and U_3 are computed locally in Benchmark 3 (the offloading ratio is zero). This demonstrates that the sensing signal is effective in suppressing E . Fig. 3(c) shows the energy consumption of Benchmark 3 is the highest while that of the proposed scheme is the lowest. This is because U_2 and U_3 are too close to E , and all data are processed locally. Compared with Benchmark 1 and Benchmark 2, the trajectory and user scheduling are optimized in the proposed scheme, which effectively reduces user energy consumption. In scenario 2, shown in Fig. 4, users are distributed in a trapezoidal shape, and each user has the same approximate distance from E . Fig. 4(a) illustrates that the trajectory of S is approximately a semi-circular shape in the proposed scheme, Benchmark 2, and Benchmark 3. This is because S will be as close to the users as possible to provide services to users. Also, due to the constraint of the maximum flight speed, after finishing the service for one user, S will choose a shorter path to fly to the following user. Fig. 4(b) depicts that, in Benchmark 3, all the users do not completely offload, and some data is still processed locally since there are no sensing signals and the secure rate for each user is relatively low, making it impossible to offload all user data. This indicates that the sensing signal is helpful for improving the secure transmission rate. Fig. 4(c) shows that the energy consumption of Benchmark 3 is the highest, followed by Benchmark 1, and the proposed scheme is the smallest. This is because Benchmark 3 failed to offload fully, resulting in significant energy consumption for data transmission and local processing. For Benchmark 1, due to the fixed trajectory, the distance from S and U_2 and U_3 is too far, resulting in a low transmission rate and high energy consumption. In scenario 3, shown in Fig. 5, users are distributed in a rectangular pattern, and E is close to U_2 . S will first fly in a straight line parallel to the positive x -axis and then return along the original path in Benchmark 1 to provide the service to all the users. One can see from Fig. 5(a) that in the proposed scheme and Benchmark 2, the trajectory of S is approximately rectangular. Through the optimization of the user scheduling and the beamforming of the sensing signal, all the users can finish the data offloading and then fly directly to the next target user. In Benchmark 3, after communication services for U_1 , S will fly directly to U_3 and U_4 . This is because U_2 is too close to E to ensure

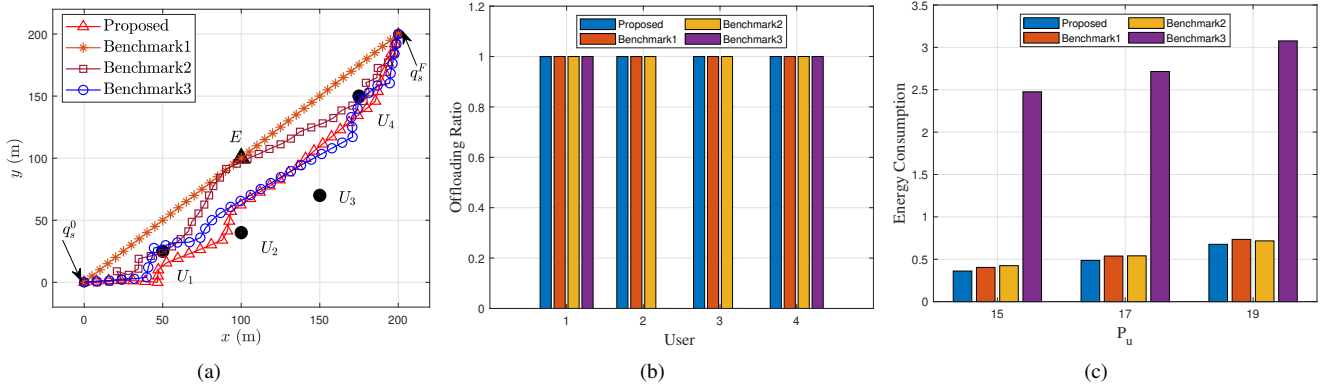


Fig. 3: Scenario 1 wherein $K = 4$ users are distributed on one side of E . (a) The optimal trajectory of S . (b) The offloading ratio of users. (c) The energy consumption of users.

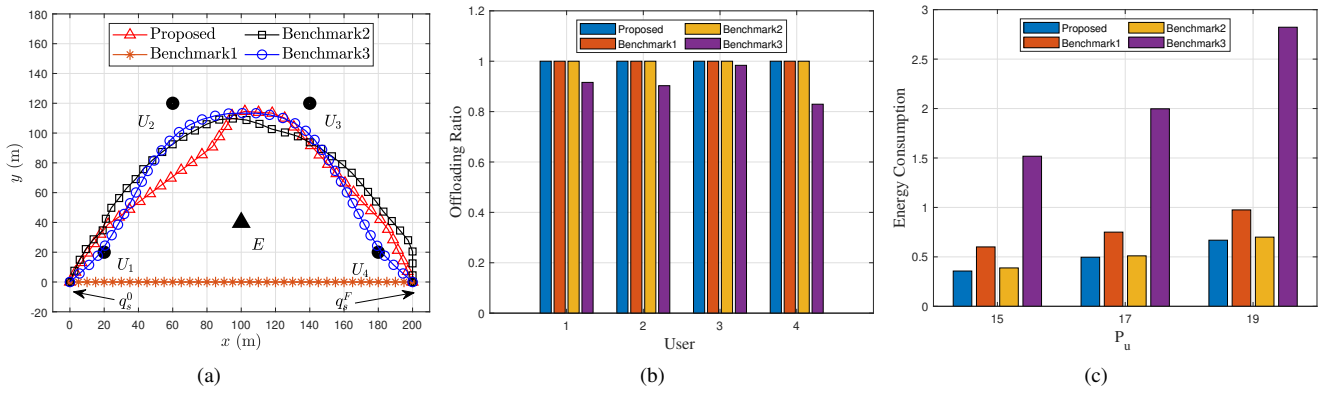


Fig. 4: Scenario 2 wherein $K = 4$ users are in a trapezoidal distribution and E is located near the center. (a) The optimal trajectory of S . (b) The offloading ratio of users. (c) The energy consumption of users.

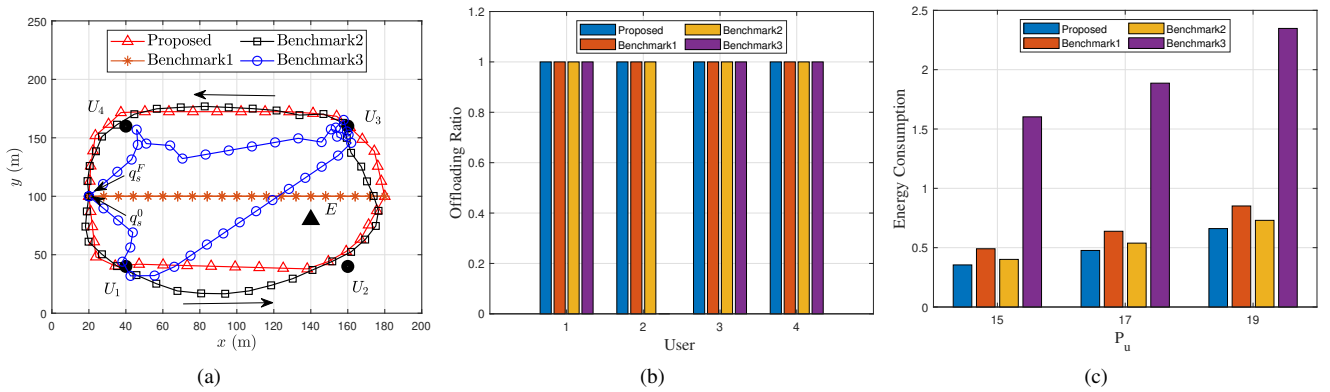


Fig. 5: Scenario 3 wherein $K = 4$ users are in a rectangle and E is located near a corner. (a) The optimal trajectory of S . (b) The offloading ratio of users. (c) The energy consumption of users.

secure offloading, which results in U_2 under Benchmark 3 only choosing all of them for local processing shown in Fig. 5(b). Similar to Figs. 3(c) and 4(c), Fig. 5(c) demonstrates the energy consumption of Benchmark 3 is the highest, and the energy consumption of the proposed scheme is the lowest. In conclusion, the results in Figs. 3-5 demonstrate in Benchmark 1, due to a fixed trajectory, although the offloading task can

be completed, the total energy consumption will be higher than that of the proposed scheme. In Benchmark 2, with fixed user scheduling and a fixed ratio of user offloading data in each time slot, the energy consumption is higher than that of the proposed scheme. For Benchmark 3, the absence of radar signal suppression for E results in a relatively low achievable secrecy rate, which leads to an excessively low offloading rate

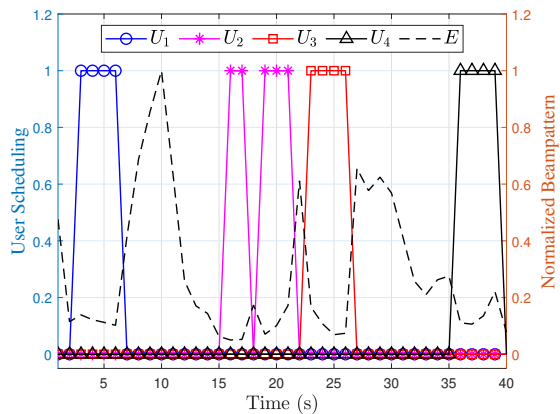


Fig. 6: The user scheduling and normalized beampattern.

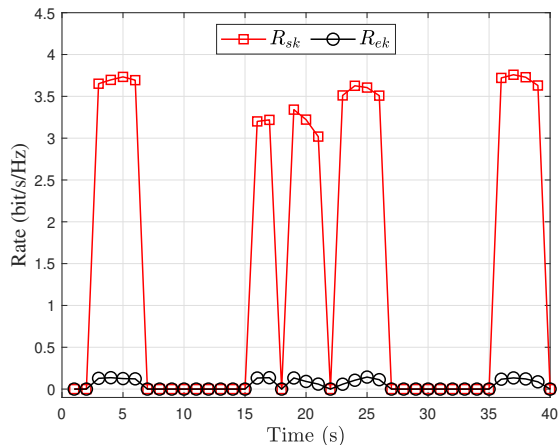


Fig. 7: R_{sk} and R_{ek} .

(scenario 2), or even zero (U_2 and U_3 in scenario 1 and U_2 in scenario 3).

Fig. 6 shows the user scheduling of the proposed scheme and the normalized beam pattern at E in scenario 2. One can observe that users are scheduled in turn to perform data offloading. The beampattern gain will decrease within the time slot when the user performs data offloading. This is because radar echoes can cause interference in communication and reduce the transmission rate. Therefore, during the time slot when the user performs data offloading, on the premise satisfying the SINR of E constraint, S will reduce the beampattern gain to reduce the influence of sensing echoes on the communication.

Fig. 7 shows the rate of S and E of the proposed scheme in scenario 2. The results illustrate that in the time slot when the user performs data offloading, the legitimate transmission rate will be much higher than the eavesdropping transmission rate. That is, by sending sensing signals, the user's security offloading rate is effectively improved.

V. CONCLUSION

This work investigated an ISAC-based UAV-assisted secure MEC system, where the UAV transmits radar signals to locate and jam potential eavesdroppers while providing uplink offload

services to ground users. By jointly optimizing the user offloading ratio, user scheduling, transmission beamforming, and UAV trajectory, the user energy consumption was minimized. To solve this complex and challenging non-convex problem, based on BCD and SCA, an effective iterative algorithm was proposed and a suboptimal solution was obtained. The numerical results testified the convergence and effectiveness of the proposed algorithm. In this work, the UAV was considered to fly at a fixed altitude and the position of the potential eavesdropper was clear. Considering 3D UAV trajectory optimization and the uncertainty of potential eavesdropping node locations will be an essential part of our future work.

REFERENCES

- [1] F. Liu, Y. Cui, C. Masouros, J. Xu, T. X. Han, Y. C. Eldar, and S. Buzzi, "Integrated sensing and communications: Toward dual-functional wireless networks for 6G and beyond," *IEEE J. Sel. Areas Commun.*, vol. 40, no. 6, pp. 1728-1767, Jun. 2022.
- [2] R. Wang, B. E. Y. Belmekki, X. Zhang, and M.-S. Alouini, "Network-level analysis of integrated sensing and communication using stochastic geometry," *IEEE Internet of Things Mag.*, vol. 7, no. 4, pp. 84-90, Jun. 2024.
- [3] Z. Wei, H. Liu, Z. Feng, H. Wu, F. Liu, Q. Zhang, and Y. Du, "Deep cooperation in ISAC system: Resource, node and infrastructure perspectives," *IEEE Internet of Things Mag.*, vol. 7, no. 6, pp. 118-125, Nov. 2024.
- [4] S. Lu, F. Liu, Y. Li, K. Zhang, H. Huang, J. Zou, X. Li, Y. Dong, F. Dong, J. Zhu, Y. Xiong, W. Yuan, Y. Cui, and L. Hanzo, "Integrated sensing and communications: Recent advances and ten open challenges," *IEEE Internet Things J.*, vol. 11, no. 11, pp. 19094-19120, Jun. 2024.
- [5] J. Mu, R. Zhang, Y. Cui, N. Gao, and X. Jing, "UAV meets integrated sensing and communication: Challenges and future directions," *IEEE Commun. Mag.*, vol. 61, no. 5, pp. 62-67, May 2023.
- [6] K. Meng, Q. Wu, J. Xu, W. Chen, Z. Feng, R. Schober, and A. L. Swindlehurst, "UAV-enabled integrated sensing and communication: Opportunities and challenges," *IEEE Wireless Commun.*, vol. 31, no. 2, pp. 97-104, Apr. 2024.
- [7] C. Deng, X. Fang, and X. Wang, "Beamforming design and trajectory optimization for UAV-empowered adaptable integrated sensing and communication," *IEEE Trans. Wireless Commun.*, vol. 22, no. 11, pp. 8512-8526, Nov. 2023.
- [8] R. Chai, X. Cui, R. Sun, D. Zhao, and Q. Chen, "Precoding and trajectory design for UAV-assisted integrated communication and sensing systems," *IEEE Trans. Veh. Technol.*, vol. 73, no. 9, pp. 13151-13163, Sep. 2024.
- [9] K. Meng, Q. Wu, S. Ma, W. Chen, K. Wang, and J. Li, "Throughput maximization for UAV-enabled integrated periodic sensing and communication," *IEEE Trans. Wireless Commun.*, vol. 22, no. 1, pp. 671-687, Jan. 2023.
- [10] X. Pang, S. Guo, J. Tang, N. Zhao, and N. Al-Dhahir, "Dynamic ISAC beamforming design for UAV-enabled vehicular networks," *IEEE Trans. Wireless Commun.*, vol. 23, no. 11, pp. 16852-16864, Nov. 2024.
- [11] X. Liu, Y. Liu, Z. Liu, and T. S. Durrani, "Fair integrated sensing and communication for multi-UAV enabled internet of things: Joint 3D trajectory and resource optimization," *IEEE Internet Things J.*, vol. 11, no. 18, pp. 29546-29556, Oct. 2024.
- [12] R. Zhang, Y. Zhang, R. Tang, H. Zhao, Q. Xiao, and C. Wang, "A joint UAV trajectory, user association, and beamforming design strategy for multi-UAV-assisted ISAC systems," *IEEE Internet Things J.*, vol. 11, no. 18, pp. 29360-29374, Sep. 2024.
- [13] X. Wang, Q. Guo, Z. Ning, L. Guo, G. Wang, X. Gao, and Y. Zhang, "Integration of sensing, communication, and computing for metaverse: A survey," *Acm Comput. Surv.*, vol. 56, no. 10, pp. 1-38, May 2024.
- [14] N. Huang, C. Dou, Y. Wu, L. Qian, and R. Lu, "Energy-efficient integrated sensing and communication: A multi-access edge computing design," *IEEE Wireless Commun. Lett.*, vol. 12, no. 12, pp. 2053-2057, Dec. 2023.
- [15] Z. Wang, X. Mu, Y. Liu, X. Xu, and P. Zhang, "NOMA-aided joint communication, sensing, and multi-tier computing systems," *IEEE J. Sel. Areas Commun.*, vol. 41, no. 3, pp. 574-588, Mar. 2023.

- [16] G. Sun, X. Wu, W. Hao, Z. Zhu, J. Li, Z. Chu, and P. Xiao, "Resource management for integrated communications, computing, and sensing (ICCS) networks," *IEEE Trans. Veh. Technol.*, vol. 73, no. 12, pp. 18719-18731, Dec. 2024.
- [17] Y. Xu, T. Zhang, Y. Liu, and D. Yang, "UAV-enabled integrated sensing, computing, and communication: A fundamental trade-off," *IEEE Wireless Commun. Lett.*, vol. 12, no. 5, pp. 843-847, May 2023.
- [18] Y. Liu, B. Zhang, D. Guo, H. Wang, and G. Ding, "Joint precoding design and location optimization in joint communication, sensing and computing of UAV systems," *IEEE Trans. Cogn. Commun. Netw.*, vol. 10, no. 2, pp. 541-552, Apr. 2024.
- [19] Y. Zhou, X. Liu, X. Zhai, Q. Zhu, and T. S. Durrani, "UAV-enabled integrated sensing, computing, and communication for internet of things: Joint resource allocation and trajectory design," *IEEE Internet Things J.*, vol. 11, no. 7, pp. 12717-12727, Apr. 2024.
- [20] C. Lei, W. Feng, P. Wei, Y. Chen, N. Ge, and S. Mao, "Edge information hub: Orchestrating satellites, UAVs, MEC, sensing and communications for 6G closed-loop controls," *IEEE J. Sel. Areas Commun.*, vol. 43, no. 1, pp. 5-20, Jan. 2025.
- [21] Z. Wei, F. Liu, C. Masouros, N. Su, and A. P. Petropulu, "Toward multi-functional 6G wireless networks: Integrating sensing, communication, and security," *IEEE Commun. Mag.*, vol. 60, no. 4, pp. 65-71, Apr. 2022.
- [22] Y. Liu, X. Liu, Z. Liu, Y. Yu, M. Jia, Z. Na, and T. S. Durrani, "Secure rate maximization for ISAC-UAV assisted communication amidst multiple eavesdroppers," *IEEE Trans. Veh. Technol.*, vol. 73, no. 10, pp. 15843-15847, Oct. 2024.
- [23] J. Zhang, J. Xu, W. Lu, N. Zhao, X. Wang, and D. Niyato, "Secure transmission for IRS-aided UAV-ISAC networks," *IEEE Trans. Wireless Commun.*, vol. 23, no. 9, pp. 12256-12269, Sep. 2024.
- [24] J. Wu, W. Yuan, and L. Hanzo, "When UAVs meet ISAC: Real-time trajectory design for secure communications," *IEEE Trans. Veh. Technol.*, vol. 72, no. 12, pp. 16766-16771, Dec. 2023.
- [25] Z. Wei, F. Liu, C. Liu, Z. Yang, D. W. K. Ng, and R. Schober, "Integrated sensing, navigation, and communication for secure UAV networks with a mobile eavesdropper," *IEEE Trans. Wireless Commun.*, vol. 23, no. 7, pp. 7060-7078, Jul. 2024.
- [26] H. Lei, X. Wu, K.-H. Park, and G. Pan, "3D trajectory design for energy-constrained aerial CRNs under probabilistic LoS channel," *IEEE Trans. Cogn. Commun. Netw.*, doi: 10.1109/TCCN.2024.3472298, 2024.
- [27] H. Lei, D. Meng, H. Ran, K.-H. Park, G. Pan, and M.-S. Alouini, "Multi-UAV trajectory design for fair and secure communication," *IEEE Trans. Cogn. Commun. Netw.*, doi: 10.1109/TCCN.2024.3487142, 2024.
- [28] P. Liu, Z. Fei, X. Wang, J. A. Zhang, Z. Zheng, and Q. Zhang, "Securing multi-user uplink communications against mobile aerial eavesdropper via sensing," *IEEE Trans. Veh. Technol.*, vol. 72, no. 7, pp. 9608-9613, Jul. 2023.
- [29] Z. Lyu, G. Zhu, and J. Xu, "Joint maneuver and beamforming design for UAV-enabled integrated sensing and communication," *IEEE Trans. Wireless Commun.*, vol. 22, no. 4, pp. 2424-2440, Apr. 2023.
- [30] X. Wang, Z. Fei, J. A. Zhang, and J. Huang, "Sensing-assisted secure uplink communications with full-duplex base station," *IEEE Commun. Lett.*, vol. 26, no. 2, pp. 249-253, Feb. 2022.
- [31] A. Khalili, A. Rezaei, D. Xu, F. Dressler, and R. Schober, "Efficient UAV hovering, resource allocation, and trajectory design for ISAC with limited backhaul capacity," *IEEE Trans. Wireless Commun.*, vol. 23, no. 11, pp. 17635-17650, Apr. 2024.
- [32] H. Lei, H. Yang, K.-H. Park, I. S. Ansari, J. Jiang, and M.-S. Alouini, "Joint trajectory design and user scheduling for secure aerial underlay IoT systems," *IEEE Internet Things J.*, vol. 10, no. 15, pp. 13637-13648, Aug. 2023.
- [33] H. Lei, J. Jiang, H. Yang, K.-H. Park, I. S. Ansari, G. Pan, and M.-S. Alouini, "Trajectory and power design for aerial CRNs with colluding eavesdroppers," *IEEE Trans. Veh. Technol.*, vol. 73, no. 12, pp. 18824-18833, Dec. 2024.
- [34] K. Meng, Q. Wu, S. Ma, W. Chen, and T. Q. S. Quek, "UAV trajectory and beamforming optimization for integrated periodic sensing and communication," *IEEE Wireless Commun. Lett.*, vol. 11, no. 6, pp. 1211-1215, Jun. 2022.
- [35] P. Stoica, L. Jian, and X. Yao, "On probing signal design for MIMO radar," *IEEE Trans. Signal Process.*, vol. 55, no. 8, pp. 4151-4161, Aug. 2007.
- [36] L. Huang, S. Bi, and Y.-J. A. Zhang, "Deep reinforcement learning for online computation offloading in wireless powered mobile-edge computing networks," *IEEE Trans. Mobile Comput.*, vol. 19, no. 11, pp. 2581-2593, Nov. 2020.
- [37] H. Lei, M. Yang, J. Jiang, K.-H. Park, and G. Pan, "Secure offloading in NOMA-aided aerial MEC systems based on deep reinforcement learning," *IEEE J. Miniatur. Air Space Syst.*, doi: 10.1109/jmass.2024.3479456, Oct. 2024.
- [38] C. Chen, J. Yao, M. Jin, and Q. Guo, "Beamforming and computing capacity allocation for ISAC-assisted secure mobile edge computing," *IEEE Wireless Commun. Lett.*, vol. 13, no. 12, pp. 3360-3364, Sep. 2024.
- [39] N. Huang, C. Dou, Y. Wu, L. Qian, B. Lin, H. Zhou, and X. Shen, "Mobile edge computing aided integrated sensing and communication with short-packet transmissions," *IEEE Trans. Wireless Commun.*, vol. 23, no. 7, pp. 7759-7774, Jul. 2024.
- [40] S. Bi and Y. J. Zhang, "Computation rate maximization for wireless powered mobile-edge computing with binary computation offloading," *IEEE Trans. Wireless Commun.*, vol. 17, no. 6, pp. 4177-4190, Jun. 2018.
- [41] Y. Zeng, J. Xu, and R. Zhang, "Energy minimization for wireless communication with rotary-wing UAV," *IEEE Trans. Wireless Commun.*, vol. 18, no. 4, pp. 2329-2345, Apr. 2019.
- [42] Q. Dan, H. Lei, K.-H. Park, G. Pan, and M.-S. Alouini, "Beamforming design for joint target sensing and proactive eavesdropping," *arXiv:2407.06521*, 2025, [Online]; <https://arxiv.org/abs/2407.06521>
- [43] Z. Yu, Y. Gong, S. Gong, and Y. Guo, "Joint task offloading and resource allocation in UAV-enabled mobile edge computing," *IEEE Internet Things J.*, vol. 7, no. 4, pp. 3147-3159, Apr. 2020.